

# ***The Quake-Catcher Network Rapid Aftershock Mobilization Program Following the 2010 M 8.8 Maule, Chile Earthquake***

**A. I. Chung,<sup>1</sup> C. Neighbors,<sup>2</sup> A. Belmonte,<sup>3</sup> M. Miller,<sup>3</sup> H. H. Sepulveda,<sup>3</sup> C. Christensen,<sup>1</sup> R. S. Jakka,<sup>4</sup> E. S. Cochran,<sup>2</sup> and J. F. Lawrence<sup>1</sup>**

## **INTRODUCTION**

Rapid detection and characterization of earthquakes is essential for earthquake early warning systems, which have the potential to alert nearby populations about the approach of potentially damaging seismic waves (*e.g.*, Allen and Kanamori 2003; Kanamori 2005). In addition, minimizing the time required to estimate the extent and amplitude of ground shaking from an earthquake is necessary for rapid deployment of emergency personnel to affected areas. A dense array of seismometers can reduce the time needed to detect an event and provide higher resolution maps of ground accelerations across a region.

Quake-Catcher Network (QCN) is a new type of seismic network that implements distributed/volunteer computing combined with micro-electro-mechanical systems (MEMS) accelerometers to record earthquakes (Cochran, Lawrence, Christensen and Chung 2009; Cochran, Lawrence, Christensen and Jakka 2009). Almost any modern computer can become a seismic station provided it has Internet access and either an internal or external MEMS accelerometer. After the initial development costs, the QCN seismic data gathering system costs less than 1% of a traditional network, thus enabling very-high-density seismic monitoring at affordable cost levels.

On 27 February 2010 an M 8.8 earthquake occurred on the subduction plate interface offshore of central Chile, with its epicenter approximately 335 km southwest of Santiago and 105 km northwest of Concepción (USGS 2010). The sole QCN accelerometer in Chile at the time, an external USB accelerometer connected to a desktop, recorded this event (see Figure 1). Although the sensor was not properly secured to the floor at the time of the earthquake, it was able to record more than 120 seconds of on-scale strong-motion shaking. Following the

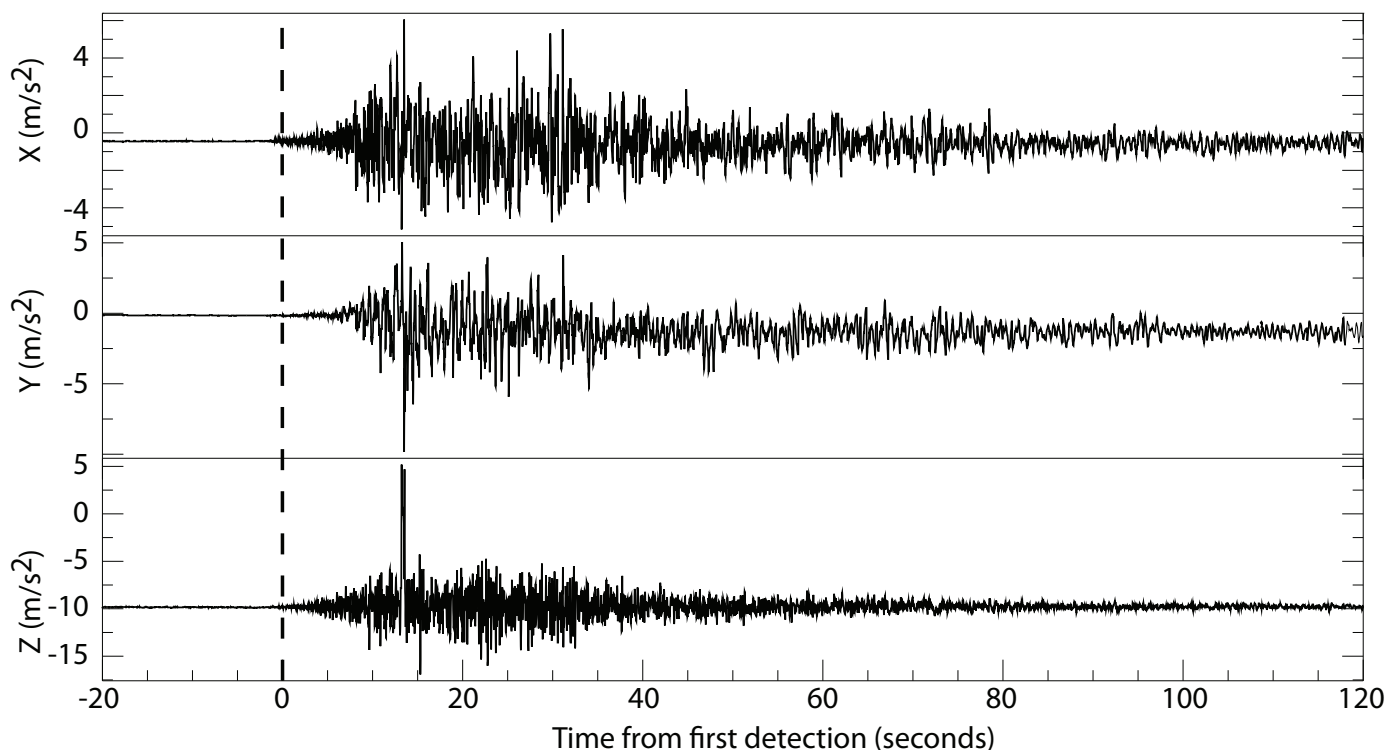
mainshock, a QCN Rapid Aftershock Mobilization Program (RAMP) was initialized in Chile and the dense network recorded a large number of aftershocks in and around the mainshock area. Here, we describe the QCN RAMP following the 27 February 2010 M 8.8 Maule, Chile earthquake.

## **DATA AND METHOD**

QCN is a distributed sensing, strong-motion seismic network that utilizes low-cost MEMS accelerometers external to desktop computers and internal to laptops. QCN runs on Berkeley Open Infrastructure for Network Computing (BOINC) open-source volunteer computing system (Anderson and Kubiatiowicz 2002; Anderson 2004) to utilize idle time on volunteer computers to monitor sensors for strong ground shaking. Accurate timing and location are necessary for reliable earthquake detection and characterization. Since QCN stations are not connected to GPS clocks, we use network time protocol (NTP) to estimate the drift on each participant computer's clock. Clock offsets are estimated every 15 minutes resulting in  $\pm 20$  msec accuracy (*e.g.*, Frassetto *et al.* 2003). Participants enter the location of their computer into a Google map interface. The building size, construction type, and sensor location are entered by the user and included in the metadata. Additional details can be found in Cochran, Lawrence, Christensen and Chung 2009; and Cochran, Lawrence, Christensen and Jakka 2009.

QCN currently supports four models of three-axis external MEMS sensors (JoyWarrior-10, JoyWarrior-14, MotionNode Accel, and O-Navi-16) that are connected to desktop computers via a USB cable. These triaxial MEMS sensors have a dynamic range of  $\pm 2$  g, resolution of 1 and 4 mg and record accelerations across a wide frequency band (typically  $0 \text{ Hz} < f < 250 \text{ Hz}$ ) (Cochran, Lawrence, Christensen and Jakka 2009; Farine *et al.* 2004; Holland 2003). Time series data are recorded at 50 samples per second. External USB accelerometers are oriented to north and mounted to the floor to ensure adequate coupling to ground motions. In addition, QCN supports two models of laptops (Apple and ThinkPad) with internal MEMS sensors. The results presented here will

- 
1. Department of Geophysics, Stanford University, Stanford, CA, U.S.A.
  2. Department of Earth Sciences, University of California, Riverside, CA, U.S.A.
  3. Geophysics Department, University of Concepción, Concepción, Chile
  4. Department of Earthquake Engineering, Indian Institute of Technology, Roorkee, India



▲ **Figure 1.** Accelerogram of the **M 8.8** mainshock recorded by a station located at the University of Concepción. The dashed line shows when the initial trigger occurred, soon after the *P*-wave arrival. Note that the sensor was not fixed to the ground and was resting on a desk at the time of the mainshock. Around 13 seconds the sensor likely falls off the desk onto the ground.

focus primarily on data recorded by floor-mounted USB accelerometers.

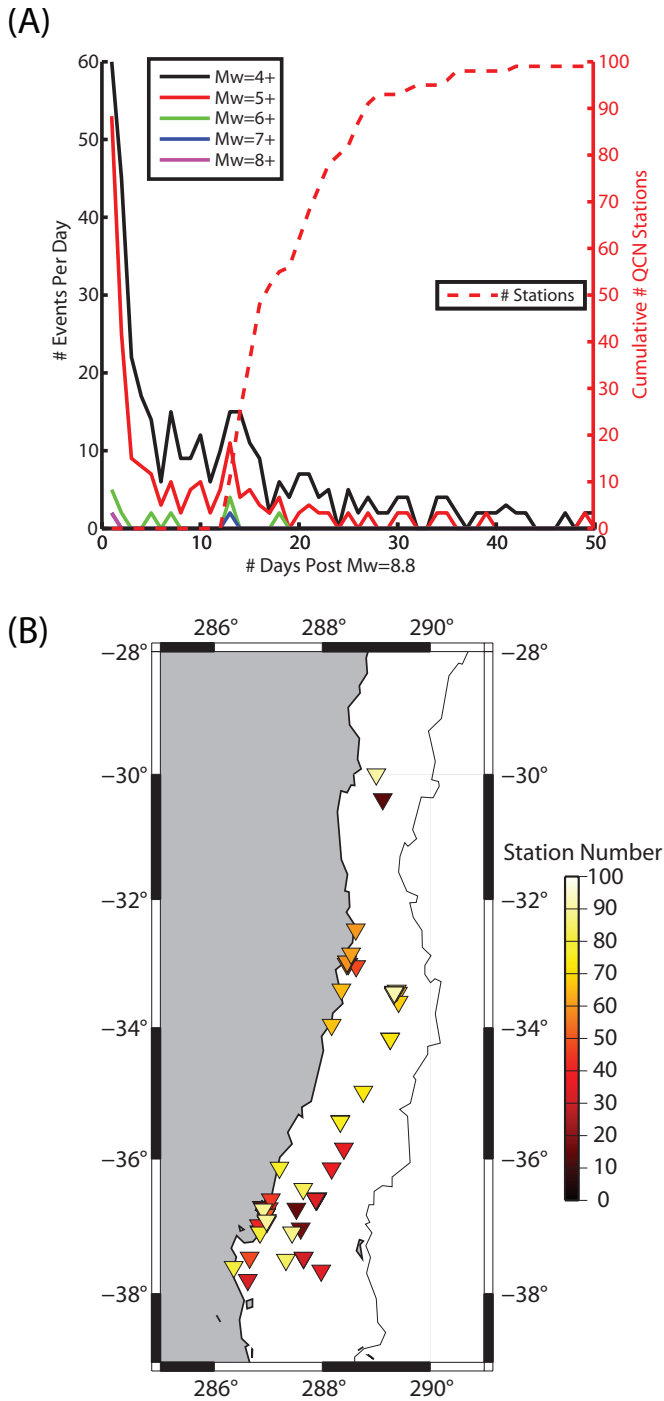
On March 8, 2010, the RAMP deployment of 100 USB accelerometers was initiated and a small team of volunteers was trained on the simple installation procedures. Participants were recruited using an online RAMP sign-up page and, following local media interviews, over 700 requests for sensors were received in roughly one week. Sensors were installed in homes, police stations, health centers, and other institutions in coordination with the national emergency authority (ONEMI). To date, QCN has 100 USB sensors and 15 laptop sensors in Chile with sensors deployed mainly in the regions directly affected by the mainshock, including a dense cluster of stations near Concepción (Figure 2). These sensors recorded continuous waveform data to ensure maximum data recovery and so event triggering and detection algorithms could be improved through retrospective testing. The abundance of large aftershocks provides a unique opportunity to examine the ability of this low-cost, distributed sensing network to rapidly detect and characterize earthquakes.

## RESULTS

Using retrospective tests on the continuous data recorded during the QCN RAMP, we tested the triggering, event discrimination, and rapid location and magnitude estimate algorithms. Figure 3 shows an example of an aftershock recorded by a large number of QCN stations located near Concepción. Most of

the sensors that recorded this event are JW-10 sensors (10-bit sensors, 4 mg resolution), but two of the stations are newer QCN sensors (JW-14 and ON-16, 14- and 16-bit sensors with 0.24 mg and 0.060 mg resolution, respectively). As expected, the higher bit sensors show dramatically lower noise levels. Using manually picked arrivals, we located this event and show that the location is similar to U.S. Geological Survey (USGS) catalog locations (Figure 3A), suggesting station locations and timing control is accurate enough to test automated event characterization algorithms.

The triggering algorithm is based on the traditional short-term average over long-term average (STA/LTA) method (*e.g.*, Vanderkulk *et al.* 1965). Here, we use a 0.1-second short-term window and a 60-second long-term window. No attempt is made to distinguish *P* and *S* waves in the initial triggering algorithm, so triggers may represent a mix of phase arrivals. Once a trigger is detected at a station, minimal information is transferred to a central server and includes station ID, station location, sensor type, three-component acceleration at the time of the trigger, significance, trigger time, and clock offset. In Chile, approximately half of the stations ( $48 \pm 13$ ) connected to the network each day and sensors are monitored for an average of about  $12.3 \pm 2.1$  hours per day (Figures 4A, 4B). Using trigger data collected between March 1 and June 1, we find that the average latencies for trigger information to be transferred to the central server from Chilean stations is five seconds, with more than 90% of the trigger information transmitted in less than eight seconds (Figure 4C).



▲ **Figure 2.** A) Number of earthquakes that occurred each day versus the number of days after the 27 February 2010 **M** 8.8 Maule mainshock for different magnitude ranges: 4+ (black line), 5+ (red line), 6+ (green line), 7+ (blue line), and 8+ (magenta line). Also shown is the cumulative number of QCN stations installed (dashed red line). The sensors arrived in Chile one week after the mainshock and deployment of the sensors began soon afterward. Almost all of the 100 stations were installed within 10 days after the deployment began. B) Locations of QCN sensors installed after the **M** 8.8 27 February 2010 Maule mainshock, colored by station number. Many of the sensors are installed in close proximity to one another and so all sensors may not be visible.

Because stations are located in high-noise environments, an individual event trigger may represent local noise not related to an earthquake; to distinguish regional ground shaking events we temporally and spatially correlate incoming triggers. We evaluate incoming triggers at 0.2 sec intervals, comparing each trigger with all other triggers that have occurred in the past 100 seconds. Triggers within 200 km are considered correlated if they occur with a time separation ( $\Delta T_{ij}$ ) less than or equal to the station separation ( $\Delta D_{ij}$ ) divided by the slowest seismic velocity,  $V_{\min}$  plus a small error,  $\epsilon$ . This takes the form:

$$\Delta T_{ij} \leq \Delta D_{ij} / V_{\min} + \epsilon. \quad (1)$$

If the average station to event azimuth is orthogonal to the inter-station azimuth, then  $\Delta T_{ij}$  should be zero. If the azimuths are parallel, then  $\Delta T_{ij}$  should equal the distance divided by the velocity. The error,  $\epsilon$ , may result from possible inaccuracy introduced by the trigger algorithm. Once at least five triggers are correlated, we make an estimate of the earthquake location and magnitude.

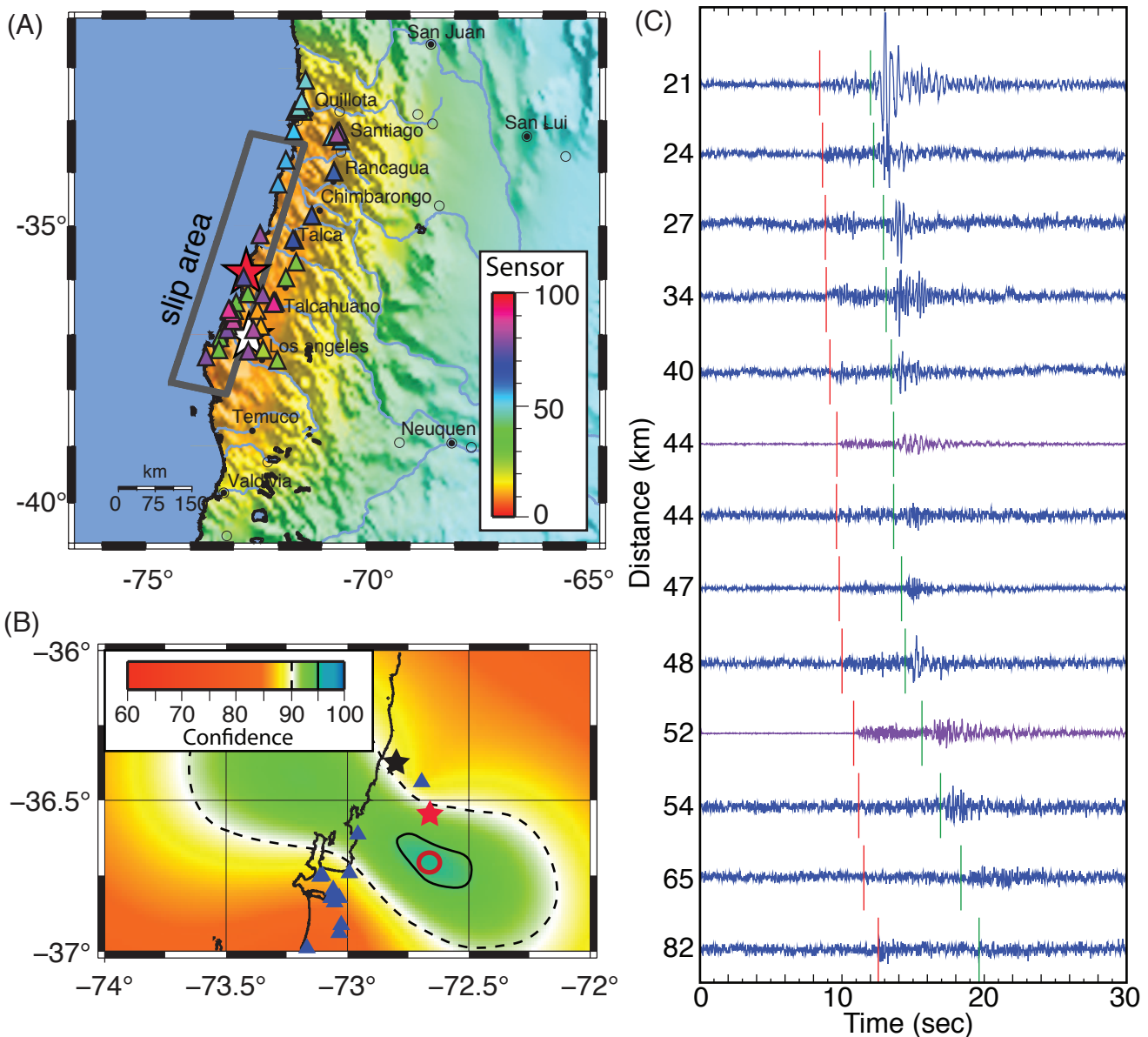
The event hypocenter is estimated by performing a three-dimensional grid search and comparing the predicted and observed relative arrivals at the stations. The initial event location is set to the station location with the earliest trigger, with the assumption that this sensor is closest to the source. An initial grid is generated that extends  $2^\circ \times 2^\circ$  in latitude and longitude with a node every  $0.02^\circ$  and a total depth interval of 300 km with nodes every 10 km. The location that minimizes the L2 misfit between observed and predicted relative travel times is identified as the low-resolution earthquake hypocenter. Using this hypocenter location, we then iterate over a second grid with grid extent and node intervals decreased by an order of magnitude.

Once the location has been estimated, the magnitude is computed using an empirical magnitude distance relationship with the acceleration vector magnitude,  $|a|$ , similar to the method of Wu *et al.* (2003) and Cua and Heaton (2007). This relationship was calibrated using three aftershocks recorded during the Chile RAMP. The equation is:

$$M_I = \frac{1}{N} \sum_{i=1}^N [a \ln(b |a|_i) + c \ln(D_i) + d] \quad (2)$$

where  $a = 1.25$ ,  $b = 1.8$ ,  $c = 0.8$ ,  $d = 3.25$ , and  $N$  is the number of triggers used. As additional triggers are logged at the server, the location and magnitude estimates of the event are updated.

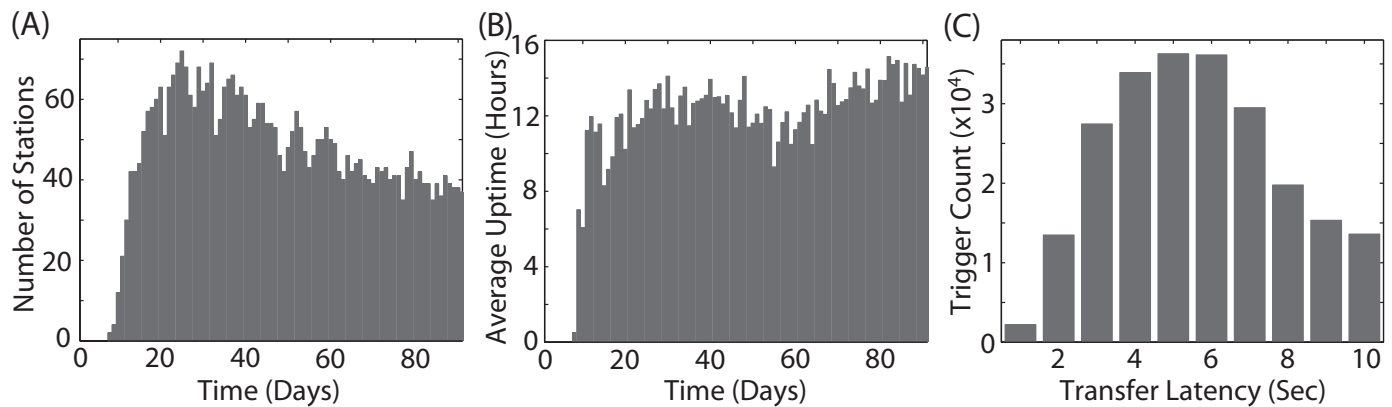
We ran a retrospective test of the automated event detection and characterization algorithms using aftershocks recorded on QCN stations around Concepción March 12–April 3, 2010. Figure 5A shows a map of 23 aftershocks identified by QCN during this 20-day period. The events are all located within the mainshock slip region, which serves as a check on the reliability of the locations. For events detected by QCN stations and also listed in the National Earthquake Information Center (NEIC) catalog (USGS 2010) we find



▲ **Figure 3.** A) Map showing the distribution of QCN stations (triangles) colored by installation date, the location of the mainshock epicenter (red star), and the approximate location of the mainshock rupture plane (gray rectangle). The background color is shaking intensity from the  $M$  8.8 mainshock (e.g., Wald *et al.* 1999) plotted over topography, with red colors indicating Modified Mercalli Intensity (MMI) X and green indicating MMI II–IV as illustrated in Figure 6. B) Comparison of USGS/NEIC catalog location and QCN estimated location for an  $M_w$  5.1 aftershock that occurred on 18 March 2010 at 01:57:33.4 UTC. QCN stations that recorded the event are shown as blue triangles and the 15-min and 7-day USGS locations are shown by black and red stars, respectively. The QCN-estimated location is shown by the red circle. Chi-squared statistical confidence is plotted as a color map with 95% and 90% confidence highlighted by the solid black and dashed black contours, respectively. C) East component time series from the stations to locate the  $M_w$  5.1 aftershock. Note the reduced noise levels on the new 14-bit and 16-bit sensors shown in purple.  $P$ - and  $S$ -wave manual picks are shown by the red and green lines, respectively.

that the magnitude estimates are very similar (Figure 5B). The uncertainty of each magnitude estimate is determined through bootstrap resampling of the trigger information. The average bootstrap uncertainty is approximately 0.45. Updated earthquake statistics are generated on a second-by-second basis as new trigger data are archived on the server, with uncertainties generally decreasing by 10–50% between iterations.

The average time needed to detect and characterize an earthquake is 27.4 seconds from the event origin time using the automated scheme described above. The fastest detection occurs within 9.4 seconds and the longest delay in detection is 59.2 seconds. Sources of latencies include: source to station wave propagation time, on-site trigger detection, time to transfer trigger information to the server, and computation time. The largest



▲ **Figure 4.** Chile RAMP statistics determined for a three-month period from 1 March to 1 June in 2010. A) Number of stations connected to the network each day. B) Average number of hours each station operated. C) Histogram showing the latencies to transfer the trigger data from the Chilean stations to the QCN central server in California.

delay in event detection for the Chile aftershock data is the time required for the seismic waves to propagate from the source to five or more stations, which is 22 seconds on average. Thus, the time required for a station to issue a trigger, send the data to the server, and compute a location and magnitude is 5.4 seconds, on average. The delay associated with updating the event characteristics is also determined by equivalent wave propagation times, on-site trigger detection, data communication, and server-side computation time, but can happen as quickly as 0.2 seconds or as late as 100 seconds after the event. Again the primary delay factor in updated characteristics is the wave propagation time.

The data collected during the QCN RAMP can also be used to provide high-resolution maps of shaking intensity and predict shaking intensity using the first few seconds of data recorded by the network. Figure 6 illustrates the high similarity between an initial attempt at providing a near real-time cyber-enabled shaking intensity map and the USGS ShakeMap (Wald *et al.* 1999). This map was calculated post-facto, but we account for all latencies including travel-time, data transfer, event characterization, and image publishing. These retrospective simulations typically provide stable shake-maps in less than 30 seconds from the aftershock origin time. The shake-maps are also rapidly updated as new trigger data arrive.

## DISCUSSION

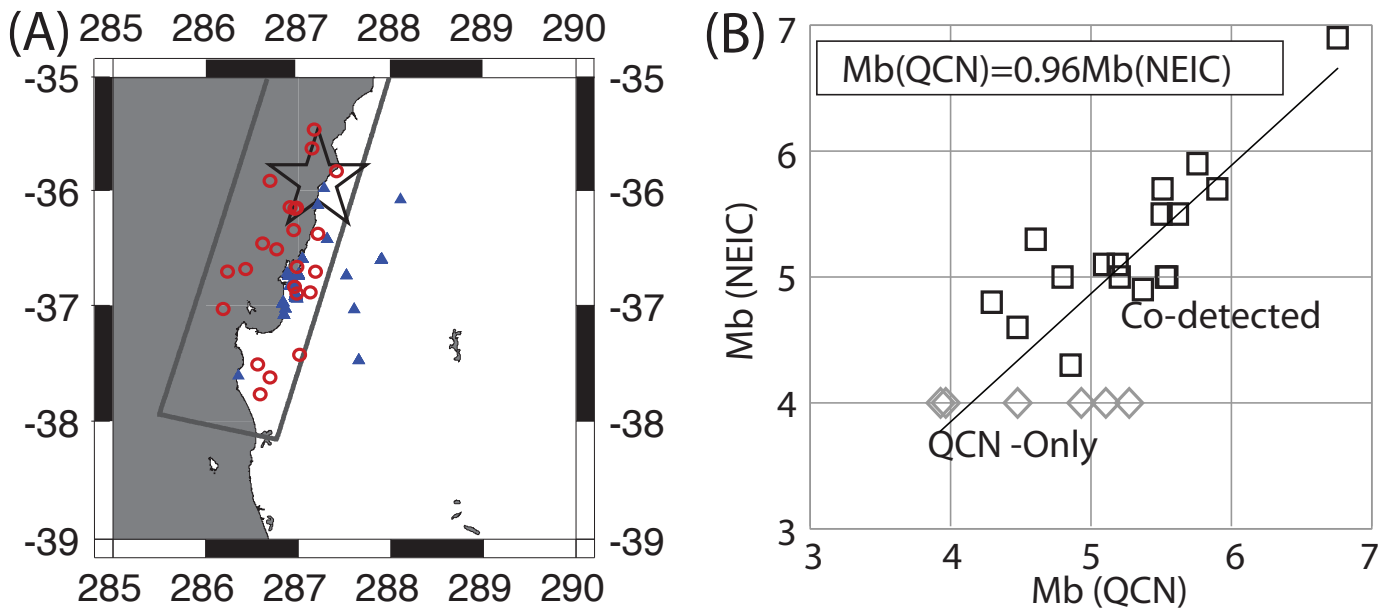
Due to the portability of the USB MEMS accelerometers and simple installation procedure, a dense real-time network of strong-motion seismic stations was installed rapidly following the 27 February 2010  $M$  8.8 Maule, Chile earthquake. Most of the 100 stations were installed within 10 days of the RAMP initiation, and we were thus able to record many of the initial, significant aftershocks. Rapid event detection and characterization is very important for directing emergency response and is critical for the future development of earthquake advanced alert systems (*e.g.*, Allen *et al.* 2009; Kanamori 2005).

As shown, we can rapidly estimate aftershock locations and magnitudes using data from the QCN strong-motion

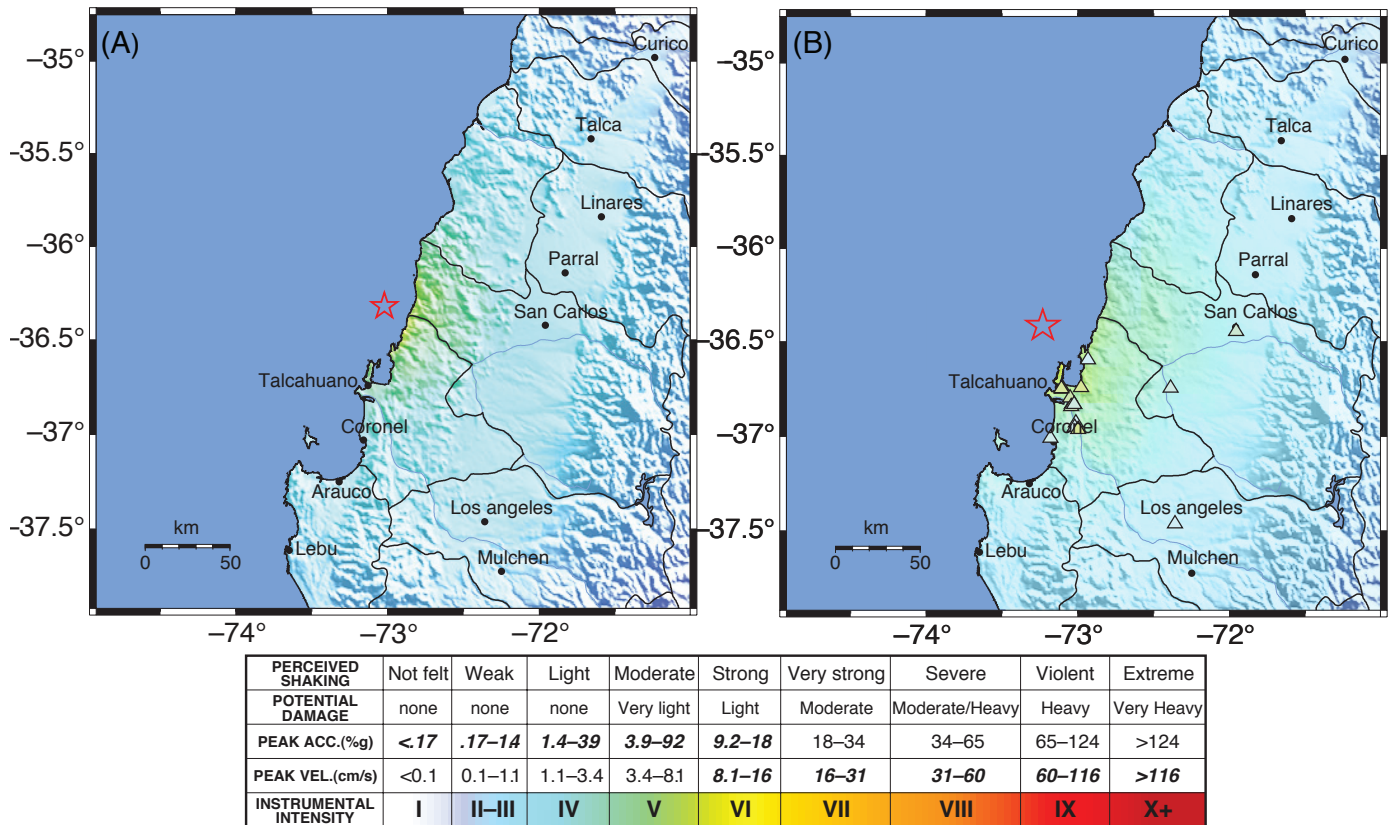
sensors. The largest delays in event detection were the source-station wave propagation times; thus, increasing the density of stations would dramatically reduce the detection time. We expect that the latest generation of sensors will further improve event detection capabilities through increased signal-to-noise ratios resulting in more reliable  $P$ -wave detections for lower magnitude ( $M < 4.5$ ) events. With little additional computation time we are able to generate maps of measured and predicted shaking amplitudes for the region around a moderate to large aftershock. Due to the higher station densities achievable with low-cost MEMS sensors and distributed sensing techniques, it is possible to examine spatial variation in ground accelerations at much higher resolution than is practical with traditional instrumentation. Detailed maps of shaking intensities could provide critical information to direct emergency responders to regions that experienced the greatest accelerations.

Installing 100 sensors in less than two weeks was surprisingly attainable. RAMP deployments that utilize MEMS sensor technology may soon be able to install 500 or more sensors in a populated region immediately following a large earthquake. Furthermore, with the arrival of the more sensitive 14-bit, 16-bit, and 24-bit accelerometers, it will be possible to record more aftershocks at greater resolution. The greatest delay in QCN's RAMP installation was in making appropriate local contacts for obtaining unrestricted access to the rupture zone. Through the combination of cyber, social, and seismic networking, QCN is rapidly overcoming this hurdle.

Having a very dense network of hundreds, or even thousands, of low-cost sensors in a region of high seismicity will provide higher resolution estimates of small-scale lateral variations in amplification effects than previously possible. This will enable us to better understand on what scales heterogeneities cause amplification, focusing, and defocusing (*e.g.*, Gao *et al.* 1996). QCN strong-motion data can also provide dense observations around a large earthquake, resulting in higher-resolution slip models and enhanced understanding of rupture properties (*e.g.*, Dreger *et al.* 2005; Jakka *et al.* 2010). ☒



▲ **Figure 5.** A) Aftershock locations (red circles) determined by a retrospective, automated event location scheme that uses trigger information from QCN stations (blue triangles) located near Concepción. Star shows the mainshock epicenter and rectangle represents the approximate mainshock slip plane. B) Event magnitudes between March 12 and April 30, 2010 for events co-detected by NEIC and QCN (black squares) and events detected only by QCN (gray diamonds). The black line is a fit to the co-detected events showing reasonable agreement between QCN-estimated magnitudes compared to NEIC catalog magnitudes.



▲ **Figure 6.** Comparison between (A) USGS ShakeMap (from USGS 2010) and (B) QCN cyber-enabled hazard map for the 16 March 2010  $M_w$  5.5 earthquake located offshore of Concepción.

## ACKNOWLEDGMENTS

This research was funded by NSF RAPID Award EAR 1035919 and NSF grant EAR-0952376. The authors would also like to thank geology and geophysics students from the University of Concepción for their invaluable assistance with deploying the sensors.

## REFERENCES

- Allen, R. M., and H. Kanamori (2003). The potential for earthquake early warning in Southern California. *Science* **300**, 786–789.
- Allen, R. M., H. Brown, M. Hellweg, O. Khainovski, P. Lombard, D. Neuhauser (2009). Real-time earthquake detection and hazard assessment by ElarmS across California. *Geophysical Research Letters* **36**, L00B08, doi:10.1029/2008GL036766.
- Anderson, D. P. (2004). BOINC: A system for public-resource computing and storage. *Proceedings of the Fifth IEEE/ACM International Workshop on Grid Computing*, November 8, 2004, Pittsburgh, USA, 4–10: <http://www.computer.org/portal/web/csdl/abs/proceedings/grid/2004/2256/00/2256toc.htm>
- Anderson, D. P., and J. Kubiatowicz (2002). The world-wide computer. *Scientific American* **286**, 40–47.
- Cochran, E. S., J. F. Lawrence, C. Christensen, A. I. Chung (2009). A novel strong-motion seismic network for community participation in earthquake monitoring. *Institute of Electrical and Electronics Engineers Instruments and Measures* **12**, 8–15.
- Cochran, E. S., J. F. Lawrence, C. Christensen, and R. Jakka (2009). The Quake-Catcher Network: Citizen science expanding seismic horizons. *Seismological Research Letters* **80**, 26–30.
- Cua, G., and T. H. Heaton (2007). The Virtual Seismologist (VS) method: A Bayesian approach to earthquake early warning. In *Earthquake Early Warning Systems*, ed. P. Gasparini, G. Manfredi, and J. Zschau, 97–132. Berlin & New York: Springer.
- Dreger, D. S., L. Gee, P. Lombard, M. H. Murray, and Barbara Romanowicz (2005). Rapid finite-source analysis and near-fault strong ground motions: Application to the 2003 *M*<sub>w</sub> 6.5 San Simeon and 2004 *M*<sub>w</sub> 6.0 Parkfield earthquakes. *Seismological Research Letters* **76**, 40–48.
- Farine, M., N. Thorburn, and D. Mougénot (2004). General application of MEMS sensors for land seismic acquisition, is it time? *The Leading Edge* **23**, 246–250.
- Frassetto, A., T. J. Owens, and P. Crotwell (2003). Evaluating the network time protocol (NTP) for timing in the South Carolina Earth Physics Project (SCEPP). *Seismological Research Letters* **74**, 649–652.
- Gao, S., H. Liu, P. M. Davis, and L. Knopoff (1996). Localized amplification of seismic waves and correlation with damage due to the Northridge earthquake: Evidence for focusing in Santa Monica. *Bulletin of the Seismological Society of America* **86**, S209–S230.
- Holland, J. (2003). Earthquake data recorded by the MEMS accelerometer. *Seismological Research Letters* **74**, 20–26.
- Jakka, R. S., E. S. Cochran, and J. F. Lawrence (2010). Earthquake source characterization by the isochrone back projection method using near-source ground motions. *Geophysical Journal International* doi:10.1111/j.1365-246X.2010.04670.x.
- Kanamori, H. (2005). Real-time seismology and earthquake damage mitigation. *Annual Review of Earth and Planetary Science* **33**, 195–214.
- USGS (2010). ShakeMap us2010txak: Offshore Bio-Bio, Chile <http://earthquake.usgs.gov/earthquakes/shakemap/global/shake/2010txai/>
- Vanderkulk, W., F. Rosen, and S. Lorenz (1965). *Large Aperture Seismic Array Signal Processing Study*. IBM Final Report, AROA Contract SD-296.
- Wald, D. J., V. Quitoriano, T. H. Heaton, H. Kanamori, C. W. Scrivner, and C. B. Worden (1999). TriNet “ShakeMaps”: rapid generation of peak ground motion and intensity maps for earthquakes in southern California (1999). TriNet “ShakeMaps”: Rapid generation of peak ground motion and intensity maps for earthquakes in southern California. *Earthquake Spectra* **15**, 537–555.
- Wu, Y.-M., T.-I. Teng, T.-C. Shin, and N.-C. Hsiao (2003). Relationship between peak ground acceleration, peak ground velocity, and intensity in Taiwan. *Bulletin of the Seismological Society of America* **93**, 386–396.

*Department of Geophysics  
Stanford University  
397 Panama Mall  
Stanford, California 94305 U.S.A.  
aichung@stanford.edu  
(A. I. C.)*